PHD RESEARCH PROPOSAL

Presented by
Eze, Kingsley Obinna

on October 10, 2024
at TECHNISCHE UNIVERSITÄT WIEN

Hyperpycnal sediment-laden river plumes in lakes: flow-sediment-bathymetry interactions (HARP)

Supervisors
Koen Blanckaert[1], Eletta Negretti[2], Julien Chauchat[2]

---

[1]Institute of Hydraulic Engineering and Environmental Hydromechanics, TUWien, Austria.
[2]Laboratoire des Ecoulements Géophysiques et Industriels (LEGI), Grenoble, France.

Abstract

Hyperpycnal (denser) river inflows into lakes bring sediments, nutrients, oxygen and contaminants which are crucial for the water quality. Due to the higher densities of hyperpycnal inflows, they abruptly descend (plunge) upon inflow and generate gravity driven underflows. This plunging is accompanied by mixing and entrainment of ambient lake waters which causes dilution of their initial density excess. The mixing is parameterized by the plunging mixing coefficient E_p and is of critical importance as it decides the fate and final destination of the matter carried by the river inflows.

This PhD project officially commenced on November 13, 2023 and builds on a preparatory research phase that suggests that E_p is affected by the geometry of the river mouth. This research presents the first laboratory attempt to affect the pathway of riverine inputs from hyperpycnal inflows into a sloping solid bottom of the ambient water by modifying the geometry, in particular the aspect ratio ($\mathrm{AR} = \frac{B_0}{H_0}$) and the lateral confinement at the river mouth. It also presents the first laboratory investigation including flow-sediment-bathymetry interactions at the near field region (region between the river mouth, the plunge location and just downstream of the plunge).

This study is realised by means of laboratory experiments in the unique Coriolis platform at LEGI (Laboratoire des Ecoulements Géophysiques et Industriels) which allows to mimic the turbulent flow and mixing processes at the Rhône inflow into Lake Geneva. This study is part of a bilateral project funded by Austrian Science Fund (FWF) and Agence Nationale de la Recherche (ANR) that also includes complementary field and numerical investigations.

Contents

List of Figures

List of Tables

List of Symbols

Symbol	Significance	Unit
U_0	Bulk inlet velocities	[m s^{-1}]
U	Layer-averaged velocity in the longitudinal direction x	[m s^{-1}]
V	Layer-averaged velocity in the transverse direction y	[m s^{-1}]
W	Layer-averaged velocity in the vertical direction z	[m s^{-1}]
$< U >$	Time-averaged velocity in the longitudinal direction x	[m s^{-1}]
$< V >$	Time-averaged velocity in the transverse direction y	[m s^{-1}]
$< W >$	Time-averaged velocity in the vertical direction z	[m s^{-1}]
u^*	Friction velocity	[m s^{-1}]
TKE	Turbulent Kinetic Energy	[m^{-2} s^{-2}]
Q_0	Inlet discharge	[m^3 s^{-1}]
$h_{u,0}$	Initial underflow thickness just downstream of the plunge	[m]
A	Cross-sectional area	[m^2]
H_0	Inlet water depth	[m]
B_0	Inlet channel width	[m]
E	Coefficient of mixing	
$\mathrm{Fr}_{d,0}$	Inflow densimetric Froude number	
$\mathrm{Fr}_{d,p}$	Plunging densimetric Froude number	
β	Bottom slope	
ADVP	Acoustic Doppler Velocimeter Profiler	
ADCP	Acoustic Doppler Current Profiler	
PIV	Particle Image Velocimetry	

The index 0 refers to inlet conditions, the index p to conditions at the plunge point and the index s to parameters along the inclined direction x_s.

1 Introduction

Research often progresses through various phases, each building on prior work to address increasingly complex questions. This introduction starts with elucidating the background and relevance of the research topic. The subsequent description of the state-of-the art is organized in two subsections. The first focuses on investigations by other researchers. The second focuses on recent contributions in the framework of a preparatory research phase done in cooperation between Technische Universität Wien (TUW) and École Polytechnique Fédérale de Lausanne (EPFL). The present research proposal is embedded in a bilateral research project titled "Hyperpycnal sediment-laden river plumes in lakes: flow-sediment-bathymetry interactions (HARP), involving TUW and Laboratoire des Ecoulements Géophysiques et Industriels (LEGI). The bilateral research project is externally funded by Austrian Science Fund (FWF) and Agence Nationale de la Recherche (ANR) under project number I 6180 (https://doi.org/10.55776/I6180). It includes the present PhD project that officially commenced on November 13, 2023 with focus on laboratory experiments (PhD-LAB), a Postdoc project with focus on the analysis of field data (Postdoc-FIELD), and a Postdoc project with focus on numerical simulations (Postdoc-NUM).

1.1 Background

Lakes are mostly fed by rivers or streams that bring water into them (inflows) and also act as sources of sediment particles, nutrients, organic matter, oxygen, contaminants (e.g., mercury, microplastics), heat and momentum. These inflows that have higher density than the receiving water bodies are termed hyperpycnal or negatively buoyant. The excess density may be due to the difference in temperature, salinity, suspended particles concentration or a combination of these.

When rivers of higher density flow into a larger body of ambient water, they displace the ambient waters and abruptly descend. The descent observed upon inflow is referred to as plunging and is evident in the disappearance of the hyperpycnal flows from the surface when observed from above (see fig. 1). The dense river inflow continues flowing on the bottom of the lake as a so-called underflow if no layer of equal density is encountered and can lift off from the bottom to form a horizontal interflow if it encounters a layer of equal density in a stratified lake (see fig. 2).

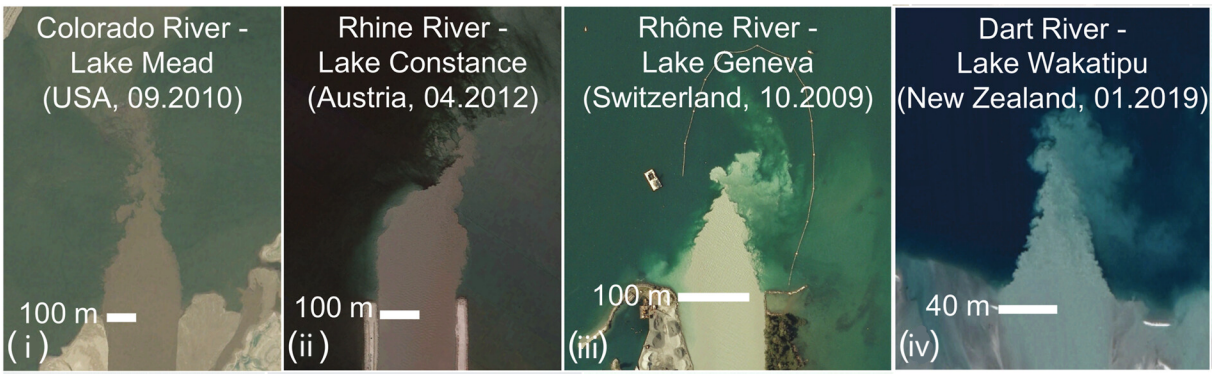

Figure 1: Field examples of unconfined hyperpycnal river plumes (modified from Thorez et al. 2024).

The pathway of hyperpycnal river flows based on the conceptual model of Fischer (1979) is illustrated in figure 2. This research focuses on the near-field region, where plume dynamics are influenced by both the river inflow and the lake. This includes the river mouth, plunging area, and immediately downstream of the plunge.

Hyperpycnal inflows are common in lakes (Fischer 1979; Alavian et al. 1992) but rare in oceans because a very high sediment load is required to overcome the density difference of $\approx$ 35 kg·m^{-3} induced by the saline ocean water (Mulder et al. 1995). Hyperpycnal inflows can be classified into confined (2d) (eg., Lee et al. 1997; Fleenor 2001; Lamb et al. 2010) and

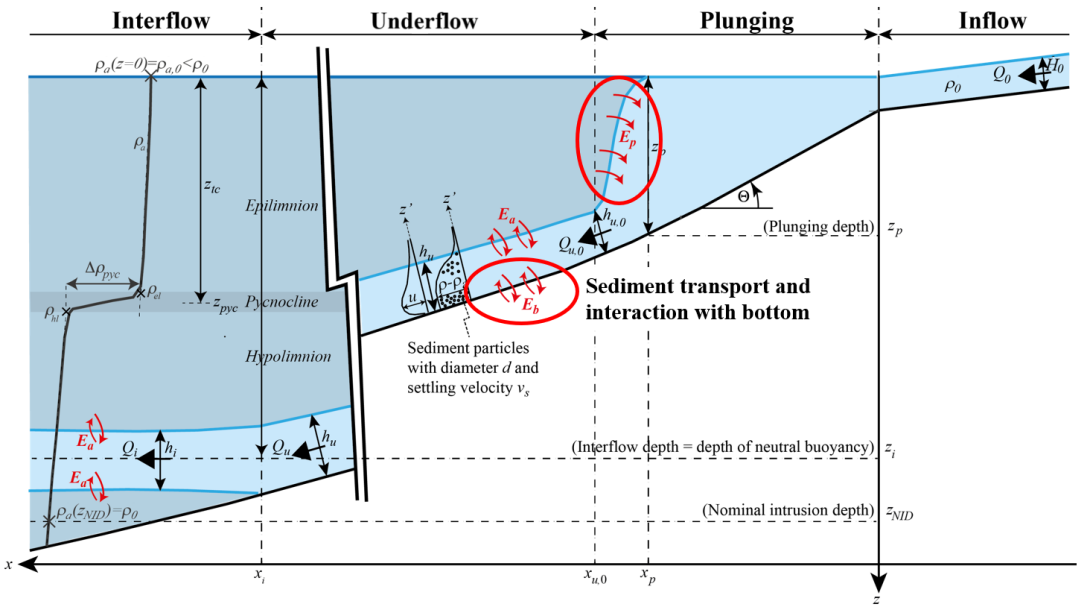

Figure 2: Existing 2d conceptual model of the evolution of a hyperpycnal riverine inflow into a lake, modified from Blanckaert et al. (2024).

unconfined (3d) (eg., Hogg et al. 2013). Unconfined inflows are characterised by the absence of lateral confinements and an abrupt change in slope at the river lake interface (see Fig 3iii). Some examples include the Lillooet River entering Lillooet Lake, Canada (Best et al. 2005), the Slims River flowing into Kluane Lake, Canada (Crookshanks et al. 2008) and the Rhône River plunging into Lake Geneva, Switzerland (Soulignac et al. 2021; Piton et al. 2022). Confined plunging on the other hand is mostly observed in laboratory flumes and lakes with a constant or uniform slope transition from the inflow and lateral confining walls (see Fig. 3i, ii).

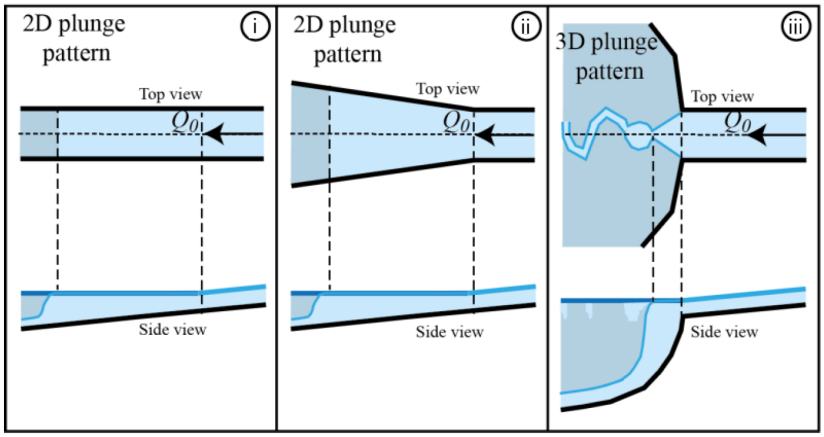

Figure 3: Scheme of hydrodynamic processes in near-field region in: (i) constant-width laterally confined geometry typical of laboratory flumes; (ii) laterally confined diverging geometry typical of dammed river; (iii) unconfined geometry typical of natural lakes. (modified from Thorez et al. 2024).

Flows resulting from the density difference between the hyperpycnal inflows and the receiving lakes are generally termed density or gravity currents. However, turbidity currents are used to describe flows with excess densities primarily due to suspended sediments. Density currents are ubiquitous in natural environments (see fig 1). Quantification of the near-field flow dynamics and the flow-sediment bathymetry interactions are of key importance as they determine the fate of nutrients, oxygen and contaminants in lakes.

The plunging which is a critical process in the near field region is accompanied by mixing

and entrainment of ambient water, which increases the volume of water entering the lake. The entrainment can be parameterized as (Akiyama et al. 1984):

$$Q_{u,0} = Q_0 + Q_a = (1 + E_p)Q_0 \tag{1}$$

$$E_p = \frac{Q_{u,0} - Q_0}{Q_0} \tag{2}$$

Here, Q_0 is the discharge of the riverine inflow, Q_a the discharge of the entrained ambient water, $Q_{u,0}$ the discharge of the underflow just downstream of the plunge, and E_p the plunging mixing coefficient (Fig. 2). The increase in discharge consequently leads to a dilution of the initial density excess. Based on mass conservation and using Equation 1, this dilution of the initial density excess can be expressed as:

$$\rho_{u,0}Q_{u,0} = \rho_0 Q_0 + \rho_{a,0}Q_a \rightarrow \rho_{u,0}(1 + E_p)Q_0 = \rho_0 Q_0 + \rho_{a,0}E_p Q_0 \rightarrow \frac{\rho_{u,0} - \rho_{a,0}}{\rho_0 - \rho_{a,0}} = \frac{1}{1 + E_p} \tag{3}$$

where ρ_0 is the density of the river and $\rho_{u,0}$ the bulk (depth-averaged) density of the underflow just downstream of the plunge. It is assumed that $\rho_{a,0}$ is constant in the surface layer where the plunging occurs. Equation 3 expresses that the density excess just downstream of the plunge is smaller than the inflow density excess by a factor $1 + E_p$.

In addition to the plunging mixing and entrainment, Fischer (1979) have also pointed out the importance of the location of the plunge, x_p (see fig. 2), and the thickness of the underflow just downstream of the plunge, $h_{u,0}$ (see fig. 2), as they define the initial conditions of the underflow downstream of the plunge. The densimetric Froude number, Fr_d, is known to be a dominant control parameter in the near-field region (Akiyama et al. 1984; Shi et al. 2022). It represents the competing influences of the inflow momentum and the buoyancy induced by the excess density and is defined as:

$$\mathrm{Fr}_d = \frac{U}{\sqrt{g'H}} \tag{4}$$

Here $g' = \frac{g(\rho - \rho_a)}{\rho_a}$, represents the reduced gravity, g the gravitational acceleration, ρ and ρ_a are the densities of the river plume and ambient water respectively, U and H the layer-averaged velocity and thickness of the river plume, respectively, and β the bottom slope.

Not all the inflowing river water plunges towards the bottom of the lake. For some sediment laden plumes, loss of excess density due to sediment deposition could cause the plume to rise vertically in a process called lofting (Hage et al. 2019; Wells et al. 2021). Although the riverine inflow is hyperpycnal, part of it "leaks" into the surface layer (see fig. 3b-iii). This surface leakage is important for the quality of the surface waters and was first observed by Fischer et al. (1983) in Lake Mead, USA.

Although the plunging, surface leakage and underflow have been identified long ago, the flow processes and flow-sediment-bathymetry interactions in the near-field region are still not fully understood and quantified. Understanding the intricate mechanisms of how hyperpycnal river inflows transport matter, mix with surrounding waters and interact with the bottom in this region is pivotal and fundamental for predicting and modelling the trajectories of diverse fluvial materials, including dissolved oxygen, heat, chemicals, biological particles, and sediment. By unravelling these dynamics, we can tentatively project how these materials may influence water quality, local ecosystems, and the morphological evolution of aquatic environments (Shi et al. 2022).

1.2 State of the art

1.2.1 Investigations by other researchers

Most previous research on hyperpycnal river plumes has focused on the underflow in the far-field region (Fig. 2) and the propagation of the head of the underflow (eg., Garcia et al. 1993; Hallworth et al. 1998; De Leeuw et al. 2016), while the near-field region remains under-investigated. Sequeiros et al. (2009) observed that a plunging open-channel inflow led to different underflow behaviour than an inflow introduced under a sluice gate at the bottom. These observations underline the complexity and importance of the hydro-sedimentary processes of the river plume in the near-field region. The current quantitative insight in the plume dynamics in the near-field region is largely based on measurements in simplified laboratory configurations. Most previous laboratory investigations were performed in constant-width quasi 2d laterally confined configurations with a flat bottom of constant slope (Fig. 3i,ii) (eg., Lee et al. 1997; Fleenor 2001; Lamb et al. 2010). It remains an open question to what extent processes in such simplified configurations are representative of their counterparts in the natural environment. This points to the need for performing field measurements (in the framework of the simultaneous complementary project by Postdoc-Field) and for performing laboratory experiments in more realistic configurations (the present project).

It has been hypothesized in the past that $\mathrm{Fr}_{d,p}$ is a main control plunging parameter and that plunging occurs at a relatively constant value of $\mathrm{Fr}_{d,p}$ (Alavian et al. 1992; Singh et al. 1971; Lee et al. 1997) similar to the hydraulic jump in open-channel flow. The body of data available to date invalidates this hypothesis and indicates that the hydro-morphodynamic processes in the near field region are complex (Fleenor 2001; Arita et al. 2008; Lamb et al. 2010) and depend on a multitude of parameters in non-confined configurations such as the geometry of the inlet channel, bottom slope of the receiving water body β and the inflow densimetric Froudes number $\mathrm{Fr}_{d,0}$.

Several laboratory studies have reported entrainment values in confined configurations with weak slope ($\mathrm{E}_p = 0.17$) (eg., Lee et al. 1997; Fleenor 2001), confined configurations with steep slope ($\mathrm{E}_p = 0.2$) (Lamb et al. 2010), flat bottom of constant slope with slightly diverging width channels ($\mathrm{E}_p = 0.68$) (Akiyama et al. 1987) and strongly diverging configurations ($\mathrm{E}_p = 3.4$) (eg., Johnson et al. 1989; Stefan et al. 1989). From numerical simulation in laterally unconfined configurations over a sloping bed, Shi et al. (2022) found $\mathrm{E}_p = 0.4$ - 0.7. Unconfined field experiments often report even larger E_p values, with Spigel et al. (2005) and Piton et al. (2022) finding values around 2–2.94, far exceeding those found in laboratory experiments of similar configurations with sloping bottom.

These researchers have mostly focused on flow and mixing processes. Much attention has not been accorded to sediment transport and morphological processes in the near field region. Most available laboratory experiments with sediment only considered suspended sediment and focused on the far-field region (García 1993; Garcia 1994; Garcia et al. 1993; De Leeuw et al. 2016). The influence of suspended sediment on the hydrodynamic processes in the near-field region has only been addressed in few experiments. For instance Lee et al. (1997) observed no influence of the presence of very fine suspended sediment with mean diameter $d_{50} = 6$ µm. Lamb et al. (2010) performed experiments with suspended sediment of $d_{50} = 21$ µm, and observed a general deposition of sediment in the near-field region but did not investigate the influence of the suspended sediment on the hydrodynamic processes.

Despite these contributions, many open questions on the flow and sedimentary processes in the near field regions persist which motivate further research. Investigations into some of these open questions started in 2017 in the framework of our preparatory research phase discussed in the following subsection.

1.2.2 Preparatory research phase

My PhD research builds on a prior research phase that involved field measurements in the framework of the PhD project of Thorez at Technische Universität Wien (TUW) and laboratory experiments and numerical simulations in the framework of the PhD project of Shi at École Polytechnique Fédérale de Lausanne (EPFL) in cooperation with Laboratoire des Ecoulements Geophysiques et Industriels (LEGI). This research phase started in 2017, was designed by the PhD supervisor Koen Blanckaert and performed in a cooperation between TUW, EPFL and LEGI.

A measurement setup was deployed at the near-field region of the inflow of the hyperpycnal Rhône river into lake Geneva. This set-up consists of remote-sensing cameras, a BLIMP (Balloon Launched Imaging and Monitoring Platform) and a boat-towed acoustic doppler velocity profiler (ADCP).

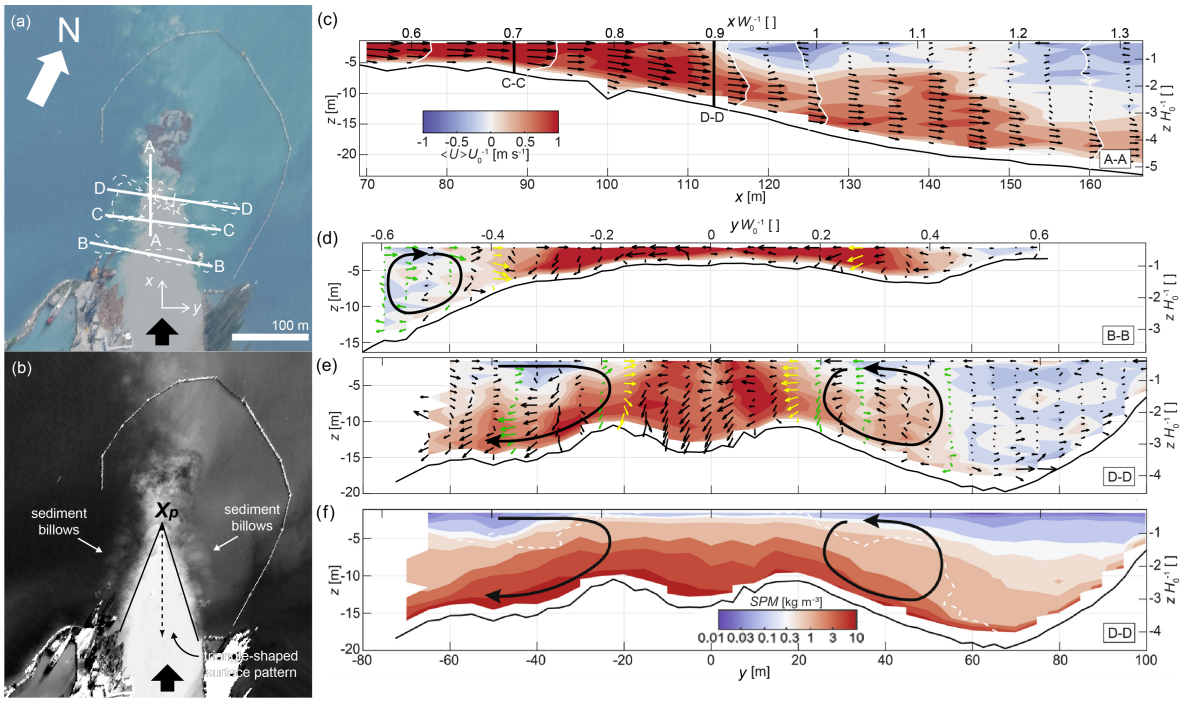

Figure 4: Field measurements of Rhône river inflow into lake Geneva on 26.06.2019 (a) surface pattern from remote-sensing cameras indicating longitudinal and transverse transects (b) Average of eight consecutive images taken during the measurements of transect B-B, gray-scaled and contrast-enhanced. This image shows the triangle-shaped, sediment-rich surface pattern and billows of sediment-rich water at some lateral distance from the triangle-shaped surface pattern. Thick black arrows indicate stream wise flow direction (c-e) ADCP-measurements and flow patterns along three transects; five velocity profiles are highlighted by white lines. In transects B-B, C-C and D-D, transverse-vertical velocity profiles shows the lateral convergence (yellow) and the secondary flow cells (green), the curved black arrows further emphasize the secondary flow cells. (f) pattern of suspended sediment concentration (SSC) derived from ADCP backscatter in transect D-D (source: modified from Thorez et al. 2024).

In the framework of the preparatory field investigation, Thorez et al. (2024) found that the triangular surface pattern (Fig. 4b) is a distinct feature of the unconfined plunging. Thorez et al. (2024) extended the conceptual model for geometrically confined 2d configurations (fig. 2) to geometrically unconfined 3d configurations (see fig. 5). They identified various flow structures such as shear layers, a return flow, lateral velocities on both sides of the plume etc. The flow structures combine to cause lateral slumping motion of the river plume and secondary flow cells at each side of the plume (Fig. 4e). He hypothesized that the observed discrepancy between the field and laboratory E_p is due to the relative sizes of the flow structures observed in both cases. Thorez et al. (2024) also reported an increase in the suspended particulate matter

(SPM) as the plunging flow erodes and transports sediments downstream. They hypothesised that the transient storage of sediment in the plunging region is important; sediment deposits in the plunging region most of the time, but it can be re-suspended during strong events and amplify the development of turbidity currents further downstream. This suggests that the plume interacts with the bed, potentially leading to morphological changes.

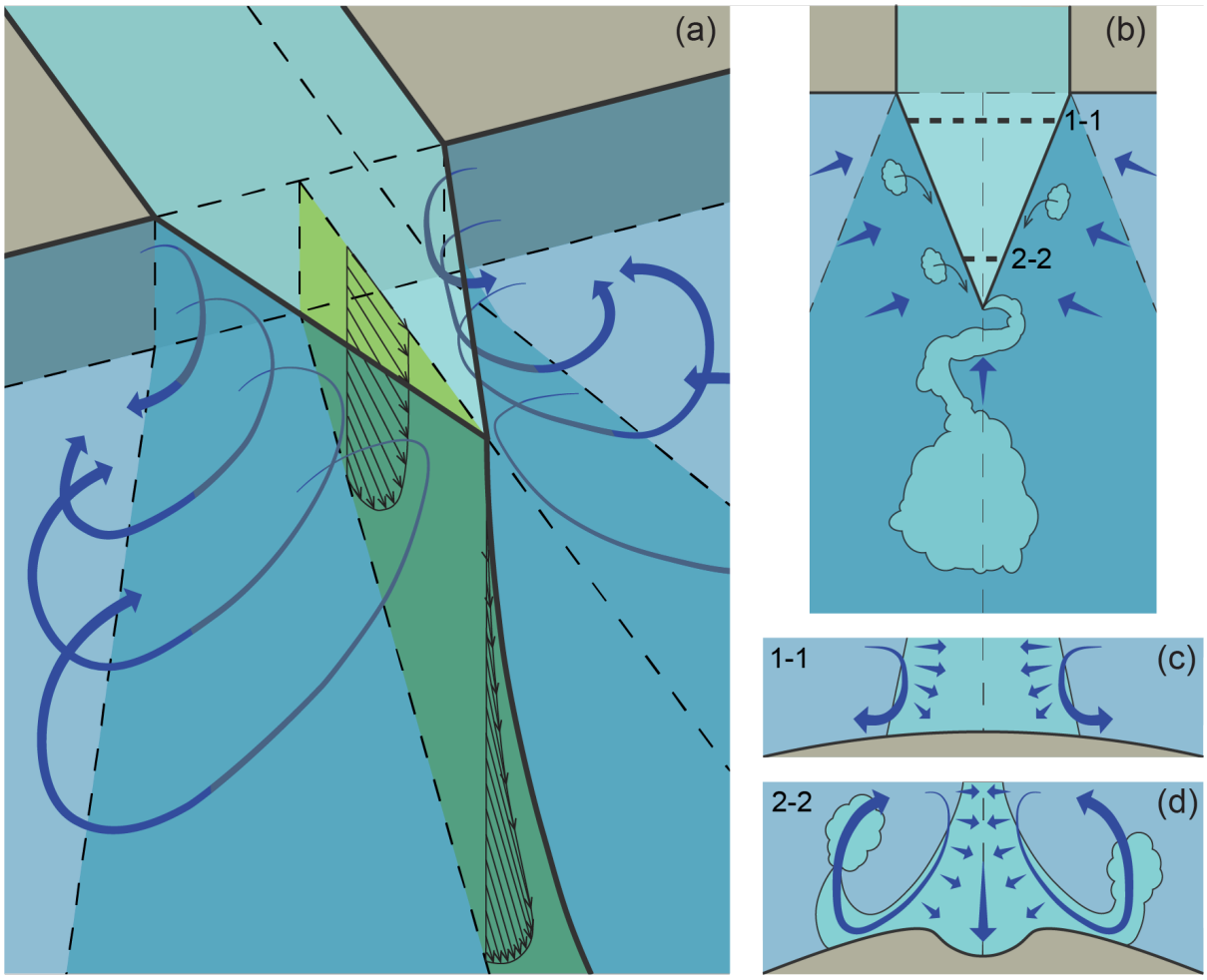

Figure 5: Conceptual model of a laterally unconfined, sediment-laden plunging river inflow. (a) 3d view. (b) Top-view. (c) Lateral-vertical transect 1-1 close to the river mouth (analogous to transect B-B in Figure 9). (d) Lateral-vertical transect 2-2 further away from the river mouth (analogous to transect D-D in Figure 9). The locations of transects 1-1 and 2-2 are indicated in panel (b). The longitudinal center line velocity profiles at transect 1-1 and 2-2 are shown in panel (a). The blue curved arrows in panels (a, c, d) indicate the suggested transport pattern of the sediment laden plume water masses outside the plume. The blue straight arrows in panel (b) indicate the suggested return current in the near-surface layer. The blue straight arrows in panels (c, d) indicate the suggested lateral flow convergence over the whole water column. Neither the thickness, nor the length of the blue arrows indicate velocity magnitudes, they exist for aesthetic purposes only. (Source: Thorez et al. 2024).

Field measurements in Lake Geneva have demonstrated that spatial patterns of suspended sediment concentration (SSC) can be derived from the ADCP backscatter with sufficient accuracy to investigate the SSC fluxes and dynamics in the river plume (Piton et al. 2022; Thorez et al. 2024). Piton et al. calibrated the relation between SSC and ADCP backscatter based on additional measurements of the particle size and SSC in individual profiles with a Laser Scattering and Transmissometry (LISST) instrument. They revealed that the coarsest sediment tends to settle out preferentially at the lateral sides of the river plume where the plume velocities are lowest. As a result, the river plume loses its density excess with respect to the ambient water

and rises vertically as clearly illustrated in Fig. 1b-iii.

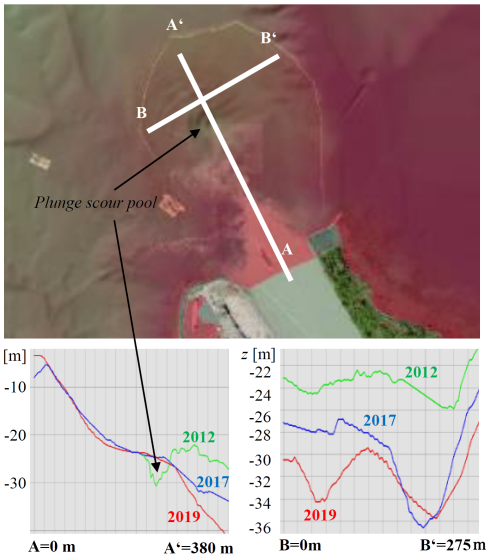

Figure 6: Bathymetric variations along AA’ and BB’ transects in the near-field region at the Rhône River inflow into Lake Geneva.

The bathymetry in the near-field region was found to be surprisingly dynamic, as indicated in figure 6 by the existence of a 7 m deep scour pool in the plunging region and the bathymetric changes of up to 10 m in the time span of 7 years. The preparatory phase on sediment transport and morphological processes concerned only the field investigations.

Additionally, a laboratory setup was developed and validated at the Laboratoire des Ecoulements Géophysiques et Industriels (LEGI)'s Coriolis platform (Fig. 7a). This platform is a unique facility that is particularly appropriate for this investigation in several aspects. First, with its diameter of 13 m and basin area of 130 m^2, the Coriolis platform allows reproducing the unconfined geometry of the Rhône inflow at a scale of 1:60. This large size of the laboratory model is required to mimic the turbulent flow and mixing processes with minimal scale effects. Second, the Coriolis platform has been specifically designed for investigations of stratified flows and has all the required technical installations. Moreover, it is fully equipped with state-of-the-art measuring technology.

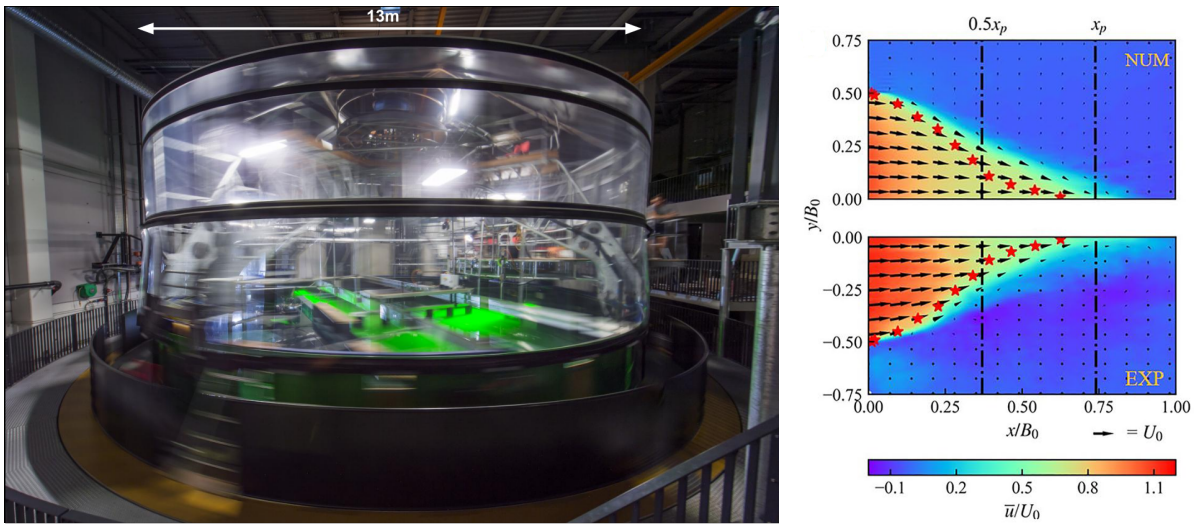

(a) (b)

Figure 7: Images from the preparatory laboratory and numerical investigations.(a) Coriolis platform (external view); (b) numerical simulations (top half) and experiments (bottom half) in horizontal planes at depth -0.5 H_0 below water surface.

Shi et al. (2022) focused on the hydrodynamics of saline inflows, i.e. inflows that are not sediment-laden. In Shi's laboratory experiments, he investigated unconfined saline plumes with constant bottom slope β and varying only the inflow densimetric Froude $\mathrm{Fr}_{d,0}$. They investigated one geometric configuration that is representative of the Rhône inflow into Lake Geneva. They found that similar to confined plunging, the main control parameters of unconfined (3D) plunging are $\mathrm{Fr}_{d,0}$ and β. However, he reported that the dynamics of confined plunging differ from those of the unconfined. Unlike the confined plunging that is hypothesised to occur when $Fr_{d,p}$ decreases to a constant value of 0.5, the unconfined plunging $Fr_{d,p}$ increases with $Fr_{d,0}$ and can get up to a

value of 1. Shi reported that the plunging mixing is influenced by secondary flow cells generated on both sides of the unconfined plume due to large density gradient between the dense plume and the ambient waters at the bottom of the slope. He found that unconfined mixing coefficient E_p is larger than its confined counterpart. Shi et al. (2022) demonstrated that the flow characteristics in the near-field region of the Rhône plume into Lake Geneva can be mimicked in the Coriolis platform and that the available instrument technology allows accurately measuring the overall flow characteristics and the relevant turbulent mixing processes. Shi's laboratory experiments were done with only one inlet channel geometry (aspect ratio $\frac{B_0}{H_0} = 25$ in a 2 m width channel) and no sediments.

In addition, Shi has also set-up a turbulence-resolving large eddy simulation(LES) 3d numerical model using OpenFoam and simulated the flow processes in the near-field region of laterally confined and unconfined geometries. He has validated the model through comparison with the data from his laboratory experiments (Fig. 7b), and used the code for enhancing insight in the flow processes (Shi et al. 2024). With his model, he studied the effect of the bottom slope on an unconfined hyperpycnal plume by extending the range of β from inclined to flat bed. He found that with larger β, the dense plume plunges closer to the river mouth. Shi also also investigated numerically the parameters related to the lateral boundary effects by extending the unconfined set-up to a confined one and with that, compared the plunging densimetric Froude number $\mathrm{Fr}_{d,p}$ and the entrainment coefficient E for both cases (Shi et al. 2022).

1.3 Research Objectives

The present investigation focuses on laboratory investigations on the near-field. It is complementary to the simultaneous analysis of field data and the numerical simulations done in the framework of the Hyperpycnal river plumes in lakes (HARP) project.

Some key points from the preparatory phase are fundamental to the motivations behind the current research. First, the laboratory and numerical investigations by Shi et al. (2022) focused on only one inlet channel width (2 m) and aspect ratio ($\frac{B_0}{H_0} = 25$), which is insufficient to fully understand the complexities of plunging dynamics, particularly since the results of the preparatory phase suggest that the pathway of riverine inputs depends primarily on the plunging mixing coefficient, and that this plunging mixing coefficient is affected by the geometry of the river mouth. This would imply that engineering measures to reconfigure the river mouth might allow affecting the pathway of the riverine inputs.

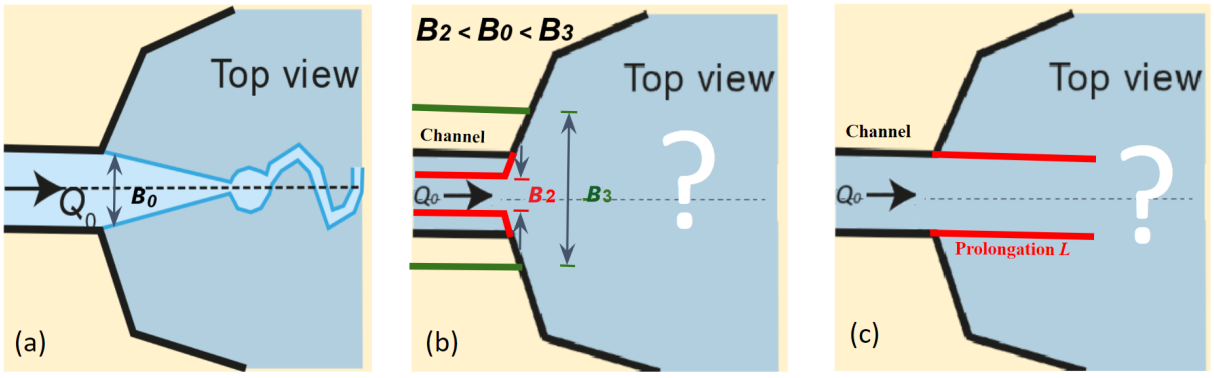

Figure 8: Schematic of the geometric reconfiguration with (a) Unconfined configuration of width B_0 (b) Increased and reduced channel widths, B_3 and B_2 respectively (c) prolongations L attached to the unconfined channel walls. Q_0 is the inlet discharge.

We hypothesize that changing the inlet aspect ratio ($\frac{B_0}{H_0}$) by reducing the channel width (B_0) (Fig. 8b) and extending the river sidewalls over the sloping lake bottom (Fig. 8c) may reduce the plunging mixing and lead to delivery of the river inputs in deeper lake waters. This would be particularly relevant for providing oxygen to the deep lake waters.

Moreover, the hypothesis of Thorez et al. (2024) regarding transient sediment storage in

the plunging region remains untested at laboratory scale. Addressing these issues is central to advancing our understanding and forms the basis for the current research.

In the first part of this PhD project, the focus is on extending the range of geometrical configurations, thereby covering the range from confined to unconfined configurations. In the second part of the PhD project, the focus is on the flow-sediment-bathymetry interactions. Specifically, the following research questions (RQ) and hypotheses (H) will be addressed:

RQ.1 How does the inlet aspect ratio ($\frac{B_0}{H_0}$) affect the hydrodynamics of plunging and in particular the plunging mixing coefficient?

- H1.1: The flow structures and mixing coefficient associated with plunging exhibit significant variation across different channel inlet aspect ratios.
- H1.2: Narrowing the inlet channel width leads to less plunging mixing and a pathway of the hyperpycnal plume that extends deeper in the ambient waters.

RQ.2 How does the extended longitudinal confinements of the inlet affect the hydrodynamics of plunging and the plunging mixing coefficient?

- H2.1: The flow structures and mixing coefficient associated with plunging exhibit significant variation when the sidewalls of the channels are longitudinally prolonged to different extents over a sloping bottom.
- H2.2: Increasing the confinement over a sloping bottom leads to less plunging mixing and a pathway of the hyperpycnal plume that extends deeper in the ambient waters.

RQ.3 What are the influence of sediments on the flow and mixing processes and how can this be quantified?

- H3.1: The presence of suspended sediments (particle weight, inertia, and concentration) does not greatly affect the turbulence characteristics in the near-field region of hyperpycnal plumes. Instead, their primary impact is on inducing lofting and surface leakage, which influence the mixing processes in the flow (section 1.1).

RQ.4 What are the dominant interactions between the flow, sediments and the bathymetry?

- H4.1: In the near-field region of hyperpycnal river plumes, sediment deposition is the dominant process for most of the time. During flood events, previously deposited sediments are re-entrained, increasing the density of the hyperpycnal plume and enhancing its sediment-carrying capacity. This cyclic pattern of deposition and re-entrainment during and between flood events leads to significant bathymetric changes in the near-field region.
- H4.2: The preferential sediment deposition at the lateral edges of the hyperpycnal plume contributes to the building up of levees. These levees further confine the plume downstream, significantly affecting the transport pathways and the fate of substances introduced by the river.

1.4 Innovation and originality

This section highlights the novel aspects of this research and its contributions to advancing the field. This work introduces new methodologies, unique perspectives, and significant advancements that set it apart from existing studies. The following points outline the key innovations and original contributions made by this research:

1. Availability of validated and optimized laboratory infrastructure thanks to preparatory phase.
2. Unprecedented coverage of the parametrical space of geometries based on the results of the preparatory investigation
3. First attempt to affect the pathway of the riverine inputs by modifying the geometry at the river mouth.
4. First investigation including flow-sediment-bathymetry interactions, which are assumed to be of primary importance based on the results of the preparatory research

2 Methodology

This research will leverage the laboratory setup developed in the preparatory phase and expand upon its results. It focuses on 2 experimental campaigns. The first campaign involves 2 sets of laboratory experiments with saline plumes (SAL). The second campaign focuses on 2 sets of laboratory experiments with sediment laden plumes (SED). The experiments SAL and the first set of SED have already been completed and the analyis of their results is underway (refer to the planning on figure 16 in section 4). In the end, the research question in section 1.3 will be addressed from the results of the laboratory experiments as detailed in table 1.

	SAL	SED
RQ.1	H1.1 H1.2	
RQ.2	H2.1 H2.2	
RQ.3		H3.1
RQ.4		H4.1 H4.2

Table 1: The research questions addressed by the experiments SAL and SED. RQ are the research questions and H represents the associated hypothesis.

2.1 Laboratory experiments of saline hyperpycnal river plumes (SAL)

The focus in these laboratory experiments with saline hyperpycnal plumes is on RQ1 - H1.1,1.2 and RQ2 - H2.1,2.2 (see subsection 1.3), as illustrated in table 1. The applied scaling laws for mimicking the flow processes at the Rhône inflow into lake Geneva are the geometric and the densimetric Froude number scaling. The Froude's scaling requires that the densimetric Froudes number are similar, $\mathrm{Fr}_{\mathrm{d,Rhône\ inflow}} = \mathrm{Fr}_{d,0}$. We have adopted the largest scale that could be built in the Coriolis flume, which resulted in a geometric scale of 1:60. This implies that the width of the Rhône inflow is 60 times the width of the laboratory channel, $W_{\mathrm{Rhône}} = 60 * W_0$. The choice of such a large scale is important to guarantee turbulent inflow conditions and in particular to mimick the development of turbulent coherent structures along the interface of the river plume and the ambient water. Based on the research of Shi et al. (2022) and Thorez et al. (2024) (subsection 1.2), the experimental set-up in the Coriolis platform was improved, and in particular the distribution and turbulence levels of the riverine inflow and the resolution of the PIV measurements.

The preparatory phase highlighted that the 3d flow patterns in the near-field region in unconfined geometries are more complex than the quasi 2d flow patterns in laterally confined geometries and characterized by a mixing coefficient E_p that is one order of magnitude larger. The SAL experiments will lead to new insight in the different dynamics of laterally confined quasi 2d and unconfined 3d plumes, in the controls that differentiate between quasi 2d and 3d mixing patterns and in the value of the plunging mixing coefficient E_p. In the preparatory phase, the influence of Fr_d has been investigated in a configuration with $B_0 = 2$ m that is representative of the Rhône inflow.

The focus of the SAL experiments was on the geometric controls (RQ1 & 2). In particular, the first set of experiments focused on the influence of the shallowness and aspect ratio (AR= $\frac{W_0}{H_0}$) of the dense inflow channel. Here, the $\mathrm{Fr}_{d,0}$ and H_0 were kept constant while reducing B_0 successively from 2 m to 1 m, 0.67 m and 0.4 m resulting in AR of 27, 13.5, 9 and 5.4 respectively. The preparatory research phase suggests that the triangular surface pattern in the near-field region is related to the lateral slumping of the higher-density water column (Fig. 4b,c). Hogg et al. (2013) and Hogg (2014) conceptualized this mechanism for laterally unconfined geometries over flat bottoms. The evolution of this surface patterns for different aspect ratios will be investigated.

In the second set of experiments, the focus was on the influence of the confinement of the dense inflow in the receiving water body. Here, for constant $\mathrm{Fr}_{d,0}$ and H_0, varying prolongation lengths of 1m, 1.5m and 2.5m as detailed in table 2 were attached to the inlet channel walls. We investigate if and how these guiding walls that prolong the riverbanks on the sloping lake bottom in the near-field region can control the transition from quasi 2d to 3d flow patterns and

therewith the degree of plunging mixing.

2.1.1 Experimental data

Flow data are obtained from PIV measurements with various instrument set-ups. In each set-up, laser sheets illuminated different sections along the vertical (z), transverse (y) and inclined (s) directions and the flow fields were realised from the particle image velocimetry (PIV) analysis of images obtained therefrom using UVMAT (http://servforge.legi.grenoble-inp.fr/projects/soft-uvmat/). UVMAT is a free Matlab toolbox (GNU General Public License) developed at LEGI. In the vertical set-up the velocity components U and W were measured. In the horizontal set-up the velocity components U and V were measured and in the inclined setup, the velocity components U_s and V_s were measured. The positions of the horizontal (H), vertical (V) and inclined (S) laser sheets are indicated in figure 9.

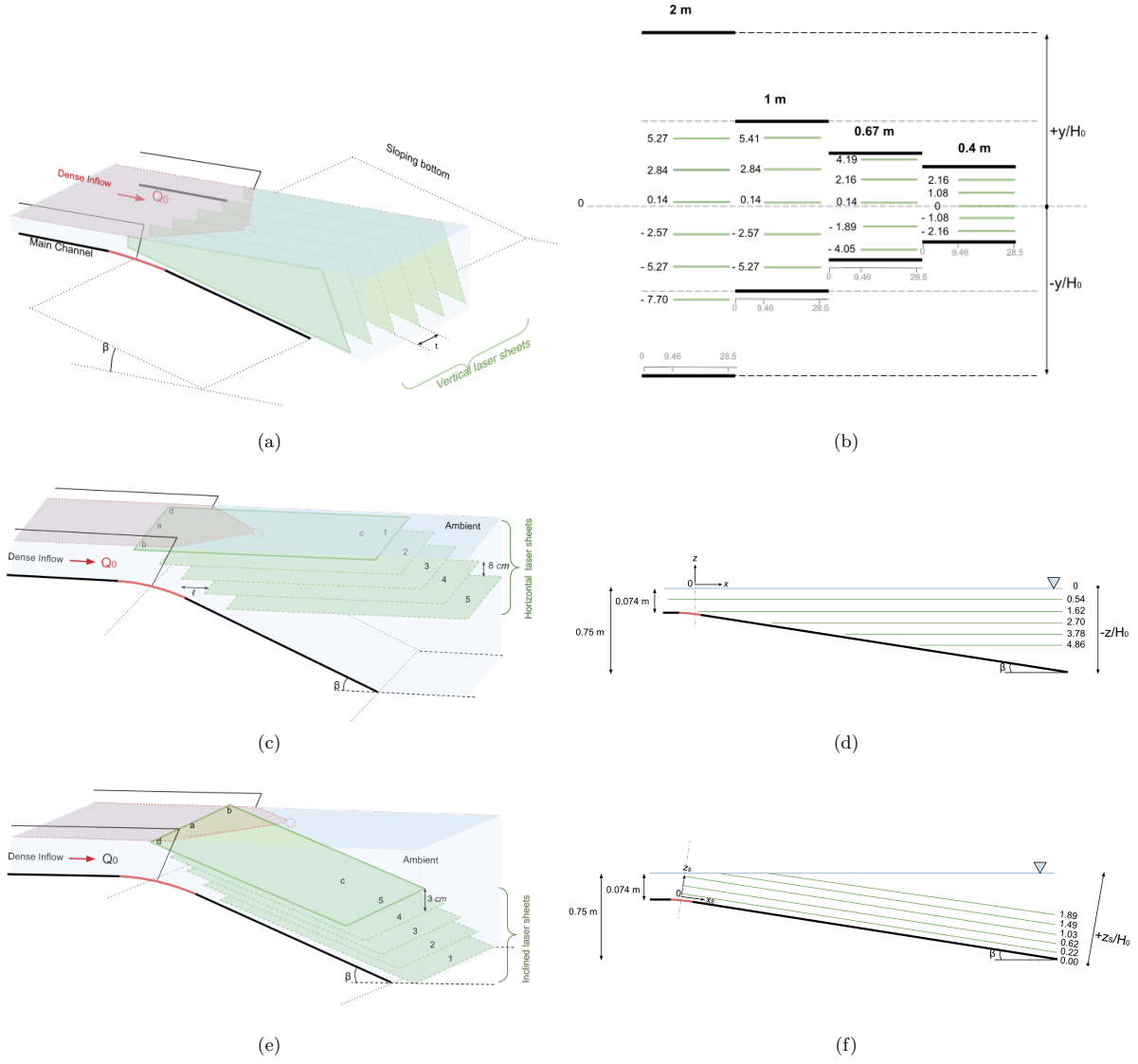

Figure 9: PIV laser positions and spacing for. a - b) Ex-V; Thick black horizontal lines show different channel widths and thick grey lines distance of the laser sheets from the channel exit at 0 and the longitudinal extents of the laser sheets c - d) Ex-H ; 5 thick green lines indicate the laser sheets at different levels with their distances from the free surface level normalised by H_0 e - f) Ex-s; 5 thick green lines indicate the laser sheets at different levels with their distances from the sloping bottom normalised by H_0.

The experiments are classified based on their PIV acquisition format. Experiment - H (Ex-H) for horizontal PIV, experiment - V (Ex-V) for vertical and Experiment - S (Ex-S) for inclined PIV parallel to the slope. Table 2 summarizes how the experiments were designed in order to investigate RQ.1 and RQ.2. To answer RQ.1 for instance, multiple experiments were performed for B_0 = 04m, 0.67m, 1m and 2m without prolongation wall. For RQ.2, the most extensive investigation on the effect of the prolongation wall was done for the configuration with B_0 =1m

The first research question RQ.1 will be tackled with experiments (H and V) from different channel widths and a single constant prolongation length while the second RQ.2 will be tackled for a constant channel width and varying prolongation lengths as in table 2.

Prolongation \ **Width**	**0.4 m**	**0.67 m**	**1 m**	**2 m**
0 m	(0.4-0-H1) (0.4-0-V1)	(0.67-0-H1) (0.67-0-V1) (0.67-0-S1)	(1-0-H1) (1-0-H2) (1-0-H3) (1-0-V1) (1-0-V2) (1-0-V3) (1-0-V4) (1-0-V5) (1-0-S1) (1-0-S2)	(2-0-H1) (2-0-V1)
1 m	(0.4-1-H1) (0.4-1-V1)	(0.67-1-H1) (0.67-1-V1)	(1-1-H1) (1-1-V1) (1-1-V2)	(2-1-H1) (2-1-V1)
1.5 m			(1-1.5-H1) (1-1.5-V1)	(2-1.5-H1) (2-1.5-H2) (2-1.5-V1)
2.5 m	(0.4-2.5-H1) (0.4-2.5-V1)	(0.67-2.5-H1) (0.67-2.5-S1)	(1-2.5-H1) (1-2.5-S1) (1-2.5-S2)	(2-2.5-H1) (2-2.5-V1) (2-2.5-V2)

Table 2: Summary of experiments based on channel width and prolongation. figures in parenthesis represent the inlet channel width [m] - longitudinal prolongation length [m]- configuration(T - trial,V - vertical, H - horizontal, S - inclined) in that order.

2.1.2 Data quality assessment

Prior to the analysis of the experimental results, a data quality check was done. This is necessary to ascertain the level of agreement in the data obtained from different experimental set-ups. The mean stream-wise velocities in Ex-H, Ex-V and Ex-S configurations were compared at the same point in space (where point velocities U from horizontal and U_s from inclined laser sheets intersect a given vertical velocity profile as shown in figure 10). The resulting velocity profile plots are in figure 11.

Good agreement is observed between Ex-V and Ex-H. However, there is no agreement with the Ex-S. This could be linked to the fact that vector resolution is required to obtain corresponding velocities with Ex-H and Ex-V from Ex-S and this requires all velocity components measured in a 3d space. Alas, only one component of the velocity U_s was measured. The good agreement observed for both horizontal and vertical data implies that the quality of the data is sufficient for further analysis.

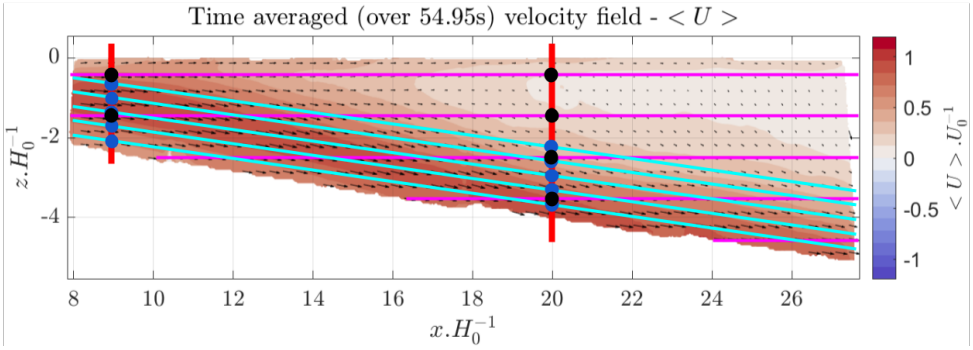

Figure 10: Spatial locations comparing longitudinal velocities for data quality assessment: Ex-H (black circles), Ex-S (blue circles), and Ex-V profile (red line); pink lines represent Ex-H laser positions and sky blue lines the inclined laser positions.

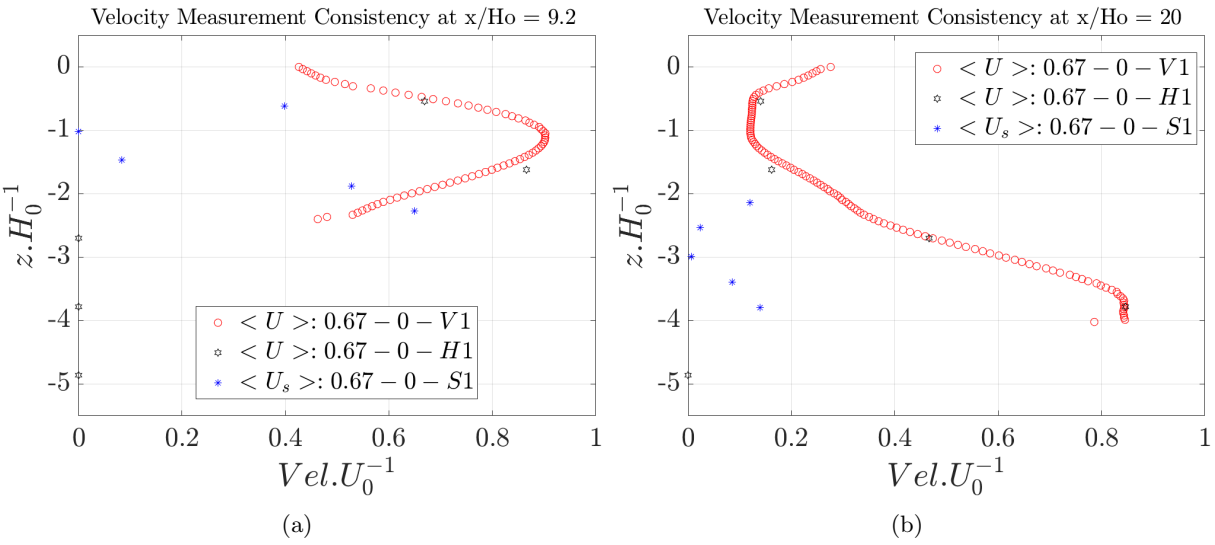

Figure 11: Longitudinal velocity plots at Ex-H (black) and Ex-S (blue) laser positions, with longitudinal velocity profile from Ex-V (red) at sections a) $x = 9.2H_0$ b) $x = 20H_0$. The plot axes represents the depth and velocities normalised respectively with the inlet water depth H_0 and mean inlet velocity U_0.

2.1.3 Verification of inflow

The inflow conditions play a crucial role in the velocity distribution inside the channel and downstream. The inflow velocity determines the turbulence characteristics and mixing behaviour of the plume while the turbulent kinetic energy (TKE) determines the intensity of turbulence. Unsteady inlet velocity across the channel width can impact the symmetry and uniformity of the flow field.

To verify the uniformity, the data from an ADV installed at the inlet channel was analysed and the mean velocities of each stationary scan in addition to the TKE were obtained. This is essential input information for the complementary numerical simulations performed by Postdoc-NUM

2.2 Laboratory experiments of sediment-laden hyperpycnal river plumes (SED)

The SED laboratory experiments will tackle RQ3 - H3.1 and RQ4 - H4.1,4.2 (see subsection 1.3), as illustrated in table 1. Besides the geometric and Froude's scaling laws described in subsection 2.1, additional scaling laws need to be respected for the suspended sediment. De

Leeuw et al. (2016) highlighted the importance of Shields scaling, which consists in reproducing the Rouse number $\frac{w_s}{u^*}$ and the particle Reynolds number $\mathrm{Re}^* = \frac{u^* d}{\nu}$. Here, ν is the kinematic viscosity of the fluid and the shear velocity is defined as $u^* = sqrt(\frac{\tau_b}{\rho})$ where τ_b is the bottom shear stress and w_s is the particle settling velocity. The Rouse number expresses the capacity of the turbulent flow to carry sediment in suspension, and Re* represents the turbulent flow characteristics near the bed. The settling velocity $w_s = \frac{(\rho_s - \rho) g d^2}{18 \nu \cdot \rho}$ indicates how fast particles will settle under gravity through the fluid.

The focus in the first set of the SED experimental campaign (trial experiments) was on adapting the Coriolis platform for sediment-laden plumes and testing of the adapted experimental set-up. The findings of the trial experiments will guide the planning and decisions for the main experiments on depositional and erosional plumes.

2.2.1 Trial experiments

The first challenge in this completed trial experiment was choosing sediment characteristics that optimally satisfy these scaling constraints and appropriate inlet conditions of discharge Q_0 and concentration of suspended sediments SSC_0 that predominantly lead to deposition or pick-up in the near-field region.

d(mm)	ρ_s	$w_s * 10^{-3}$(m s^{-1})	Re*	τ*	Rouse No($\boldsymbol{P}$)	$u^*.w_s^{-1}$	Transport rate (m^3 s^{-1})
0,3	1040	1,50	0,57	0,87	0,37	6,67	1,04E-05
0,2	1200	3,20	0,87	0,26	0,79	3,13	2,84E-08
0,3	1200	6,40	2,60	0,17	1,58	1,56	2,22E-07
0,4	1200	10,00	4,81	0,13	2,47	1,00	4,71E-07
0,6	1200	17,60	11,46	0,09	4,35	0,57	5,98E-06

(a)

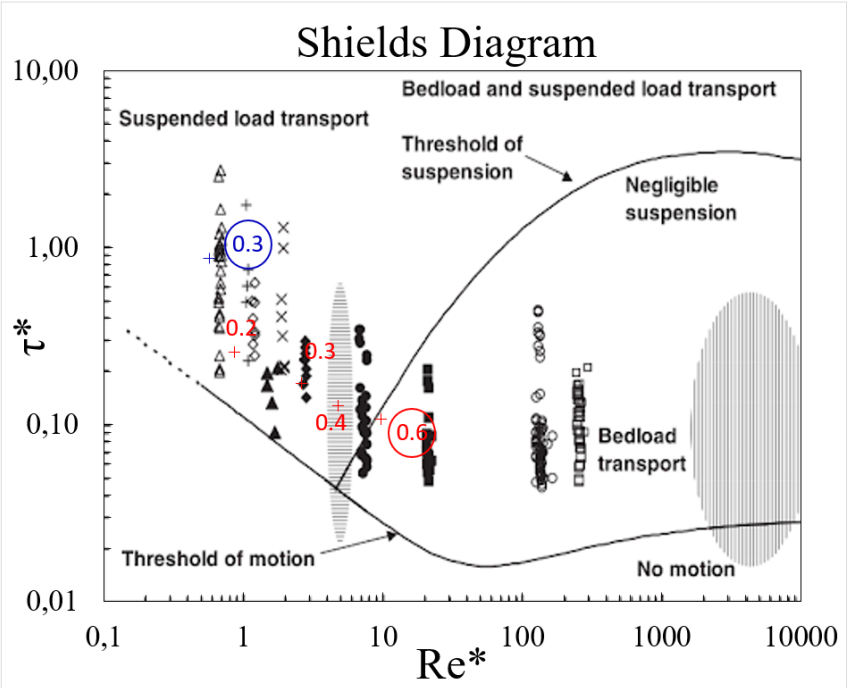

(b)

Figure 12: Sediment properties used for trial experiments in the first experimental campaign. a) Table of sediment properties b) Sediment properties plotted over shields diagram of Sequeiros et al. (2010): Particle sizes within circles represent those tested both theoretically and experimentally (in mm), while those without circles indicate sizes tested only theoretically, in blue is the polystyrene particle and red are the PMMA (polymethyl methacrylate) particles.

The trial experiments were done with PMMA (polymethyl-methacrylate) and lightweight polystyrene plastic particles. The investigated range of particle sizes d [mm], the fall velocity w_s [cm s^{-1}], the shields and the Rouse numbers are shown in figure 12a. The shields number $\tau^* = \frac{\rho u^{*2}}{(\rho_s - \rho)gd}$ represents the capacity of the flow to erode the bed, where d is the particle diameter.

Two flow types were investigated with varying particle diameters; flows with density difference due to the combined effect of salinity and particles and those due to particles alone. The trial experiments were conducted with 1m width channel and no prolongation for constant $\mathrm{Fr}_{d,0}$ and H_0. The introduction of particles increases the fluid turbidity and interfere with the accuracy and effectiveness of the measurements with the optical PIV methods. This necessitated the use of an acoustic doppler velocimeter profiler ADVP which ensured the measurement of the velocity profiles (U, V, W) in one vertical profile as the effect of the excess density on the speed of sound is relatively minor (Best et al. 2001). Surface patterns in the near-field region were measured with a standard RGB camera and velocities derived with Particle Image Velocimetry (PIV) techniques. Shi et al. (2022) used similar cameras set-up to measure surface patterns in his laboratory experiments. An equivalent field set-up is the BLIMP (Balloon Launched Imaging and Monitoring Platform) used by Thorez et al. (2024). The bathymetric changes were determined using an optical laser scan technique involving high resolution laser sheets and camera (see fig. 13a). This optical technique is similar to those used by Sequeiros et al. (2010) in his laboratory investigation of turbidity currents.

Preliminary analysis before the trial experiments show that the shields number τ^* of all the particle sizes (see fig. 12a) fall above the threshold of motion as shown in figure 12b implying that all the particles will move. However, only the 0.6 mm PMMA particles lie in the bedload transport regime and will only move along the bed. This is corroborated by its highest Rouse number (> 2.5) indicating that the settling velocity (w_s) of sediment particles dominates over the turbulence effects ($u^* = 1$) and that particles are more likely to settle to the bed rather than stay suspended in the flow. The remaining particle sizes fall within the suspension regime, with the 0.3 mm particles exhibiting the greatest suspendability.

Since deposition and pickup is desired in the near field region, representative sample sizes (0.3 mm and 0.6 mm) were chosen for the experiments to capture the extremes of particle motion and their concentrations estimated using the transport rate (fig. 12a) computed from Ackers and White model (Ackers et al. 1993). During the experiments, slight movements were observed along the bed For the 0.6 mm PMMA particles. The polystyrene particles exhibited more suspension judging by a huge sediment cloud at the onset of the experiment (see figure 13b). There was more deposition at the plunge point and polystyrene particles were picked up when the velocity increases again just downstream the plunge point. These characteristics are in agreement with the potential particle properties required for the main experiments.

In general, we demonstrated from the SED trial experiments that the 0.3 mm polystyrene particles are the most suitable choice for the main SED experiments as they favour deposition and pickup in the near field region. Additionally, we validated the experimental setup for bathymetric monitoring and tested the instrument (ADVP) set-up in preparation for the main experiments.

2.2.2 Depositional-erosional experiments

The focus in the second set of this campaign is on experiments with depositional and erosional hyperpycnal river plumes, with emphasis on the flow-sediment-bathymetry interactions (RQ4). In line with RQ4-H4.1,4.2, we plan two series of experiments (see figure 16 for timeline). The first will be performed for relatively low conditions of Q_0 and SSC_0 that predominantly cause sediment deposition in the near-field region. These experiments will be of long duration, i.e. they will consist of a series of repetitions of shorter duration. The second series of experiments will be performed for high conditions of Q_0 and SSC_0 that represent a short-duration flood event. Under such conditions, it is expected that sediment is picked up from the bottom and amplifies the density excess of the hyperpycnal plume (refer to RQ4-H4.1). In parallel, con-

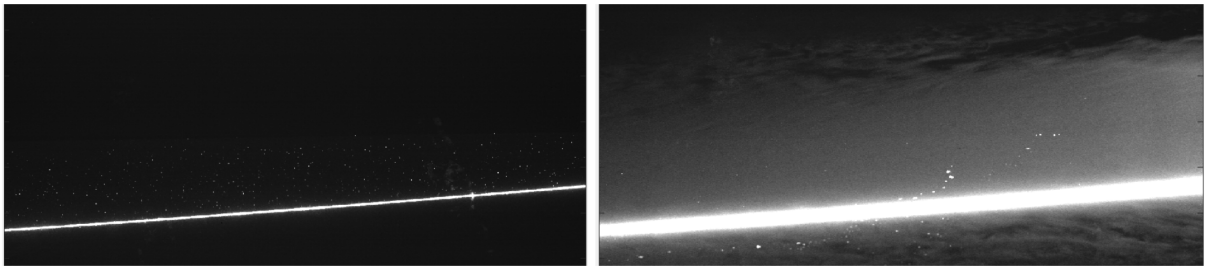

(a)

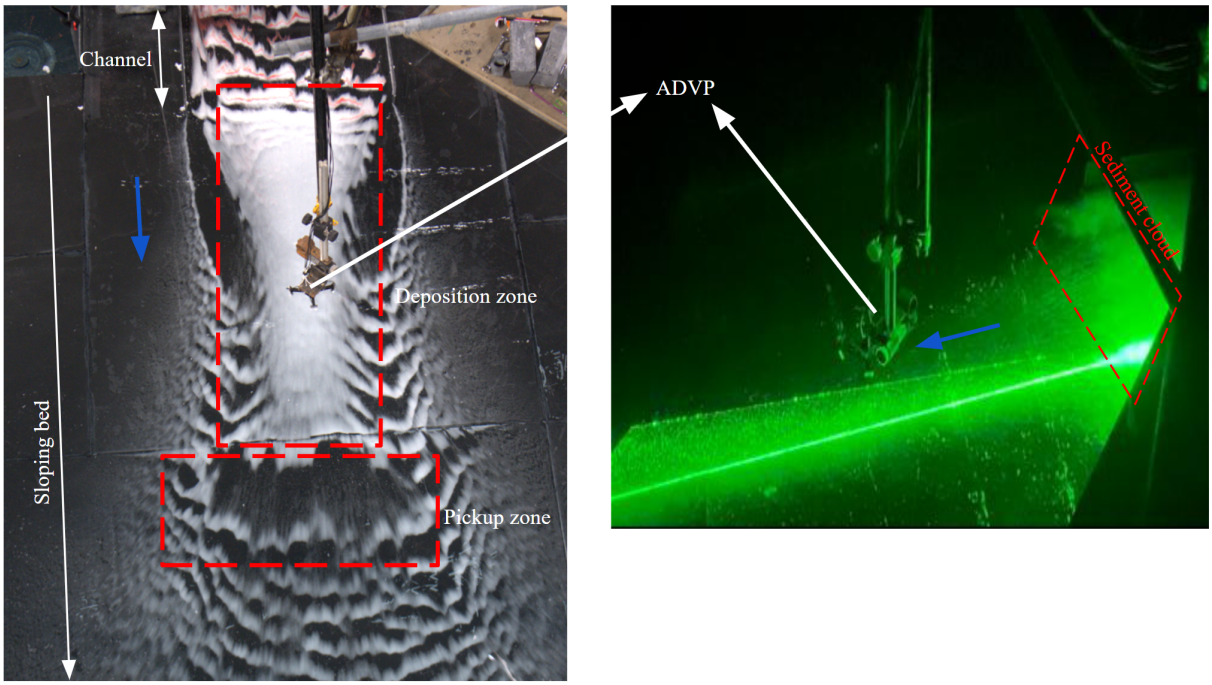

(b)

Figure 13: Preliminary observations from the sediment laden plume (test) experiments. a) Left: Pre-experiment bed scan. Right: Post-experiment bed scan. b) Left:post experiment plan view of bed structure. Right: Laser sheet (green slice) during experiment. The sediment cloud is marked by the red dashed lines and blue arrows indicate the streamwise directions

tinuous measurements will be performed of surface patterns and profiles of velocity (U, V, W) in relevant locations within the plume body with a set of Acoustic Doppler Velocity Profilers (APVP). The knowledge of sediment size allows extracting SSC from Acoustic Doppler Velocity Profiler (ADVP) backscatter data without the need for additional calibration measurements. The obtained results will be compared to measurements in saline plumes in order to investigate the influence of the sediment on the flow hydrodynamics and mixing processes (RQ3-H3.1). Additionally, the lofting and surface leakage processes will be examined using a slightly positively buoyant inflow with respect to the ambient, to determine the conditions under which they occur or are absent in our setup.

3 Deliverables

The following deliverables will contribute to the advancement of knowledge and the dissemination of research findings.

1. Open access data bases: The research data generated during this project will be made publicly available through publication in relevant open-access scientific journals, ensuring that the data is easily identifiable via a standard and unique Digital Object Identifier (DOI). All publications stemming from this project will be freely accessible to the public for transparency, reproducibility, and wider dissemination of the research findings.

2. Scripts for data treatment: Similarly, the scripts used for data treatment and analysis will be made available through open-access repositories, allowing other researchers to replicate, validate, and build upon the work. These scripts will be documented and shared with appropriate licenses to encourage re-use and collaboration.

3. Seminars and conferences: Participation in seminars, workshops, and international congresses will also be a key deliverable. These events will provide the valuable platforms to present this research, engage with peers, and receive constructive feedback, contributing to the wider dissemination of the project's findings. Where possible, presentations and proceedings will also be shared through open-access platforms.

4. Scientific papers: In addition to the PhD thesis, the following three papers are proposed for this project. They will be published in open-access scientific journals, ensuring broad accessibility and compliance with open-access mandates. More detail on the proposed papers is given in the following subsection

3.1 Proposed papers

Paper 1: Effect of inflow aspect ratio $\frac{B_0}{H_0}$ on the hydrodynamics of plunging

Kingsley Eze[1], Antonio Ammendola[3], Giamagas George[2], Stan Thorez[1], Eletta Negretti[2], Julien Chauchat[2], Koen Blanckaert[1].

[1]Institute of Hydraulic Engineering and Environmental Hydromechanics, TUWien, Austria.
[2]Laboratoire des Ecoulements Géophysiques et Industriels (LEGI), Grenoble, France.
[3]Department of Mathematics, Computer Science and Geosciences, University of Trieste, Italy.

This paper will address the first research question (RQ.1) and accompanying hypothesis. It will investigate the evolution of the plunging parameters in the near field region under changing channel widths. The entire width of the channel is consistently modified at constant inlet depth across different runs of experiments (SAL) from 0.4 m to 2 m as detailed in table 2. Preliminary analysis of the experimental data is presented in figure 14. It includes PIV measurements with spatial resolution with 0.25 cm grid spacing for the vertical scans in both x and z axis and 0.72 cm for the horizontal scans in both x and y axis. The images in figure 14 show contour and quiver plots of the velocity fields obtained for different inlet channel width and aspect ratios (AR = 5.4, 9, 13.5 and 27) in unconfined configurations. Inside the channel, the flow characteristics of narrow and wide channels differ, as the former is predominantly three-dimensional, while the latter behaves as two-dimensional in the central region, where the influence of the side walls is minimal (Shinneeb et al. 2021). These differences may proceed to affect the flow downstream. Variations can be observed in the flow fields with progressively narrowing triangular surface pattern as the width decreases in figure 14b.

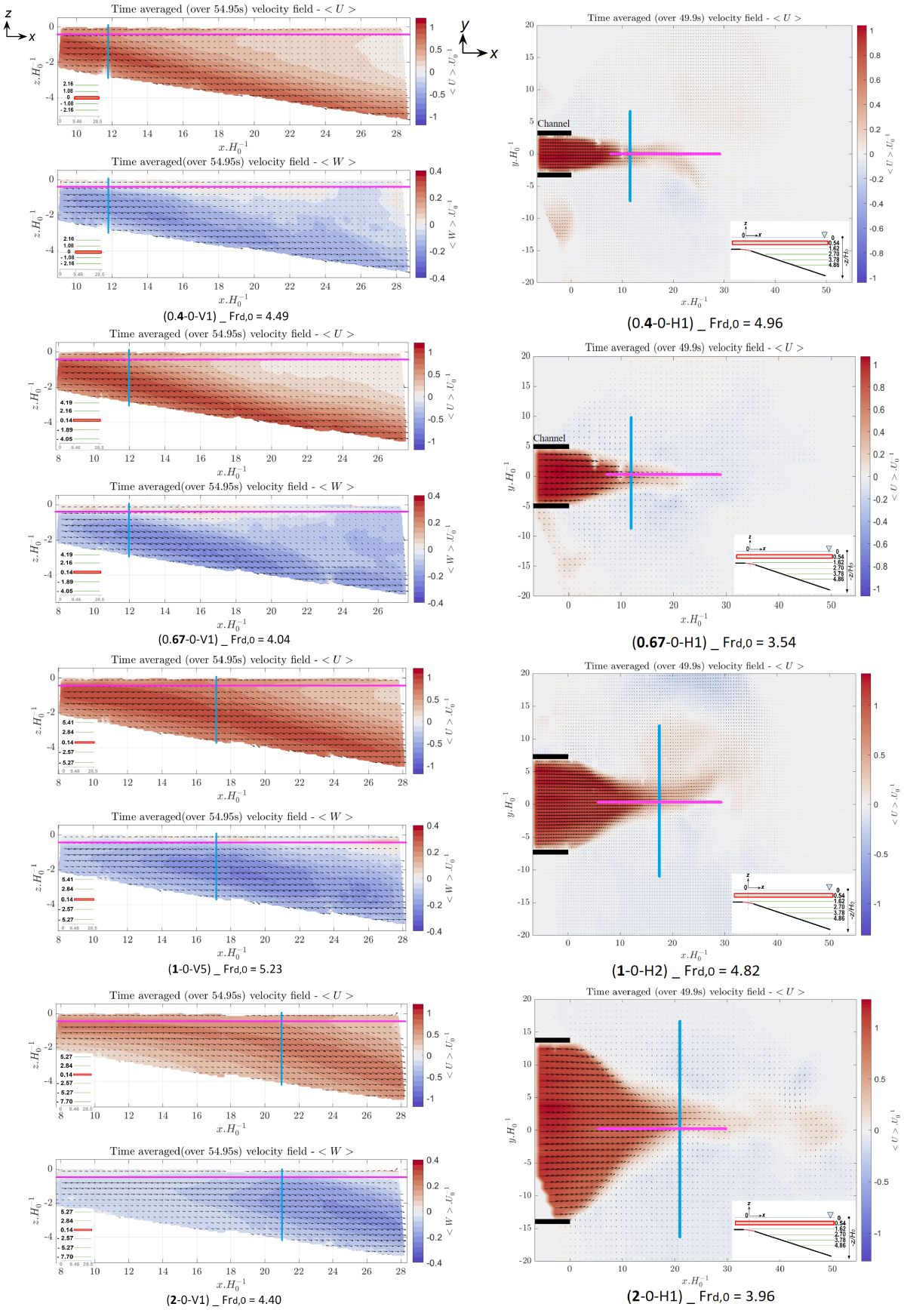

Figure 14: Typical velocity fields for 0.4 m, 0.67 m, 1 m and 2 m inlet channel widths respectively from a) Ex-V b) Ex-H. Thick black line represent the extents of the channel, green lines are the laser positions with red box indicating the current scan position, light blue lines mark the plunge locations and pink lines represent horizontal laser scan positions on the vertical(Ex-V) slice and vice versa.

As the width increases, there is gradual stream wise growth in the length of the low velocity zone marked by the decreasing negative vertical velocity W at the flow's lower boundary in figure 14a. As observed by Shi et al. (2022), the low velocity zone is especially prominent in the 2 m width channel (2-0-V1). A comprehensive analysis is underway to uncover the reasons for these differences.

Paper 2: Effect of confinement on the hydrodynamics of plunging

Kingsley Eze[1], Giamagas George[2], Stan Thorez[1], Eletta Negretti[2], Julien Chauchat[2], Koen Blanckaert[1].

[1]Institute of Hydraulic Engineering and Environmental Hydromechanics, TU Wien, Austria.
[2]Laboratoire des Ecoulements Géophysiques et Industriels (LEGI), Grenoble, France.

This paper will focus on addressing the second research question (RQ.2) and its associated hypothesis, providing an in-depth analysis on how the longitudinally extended lateral confinements affects plunging of initially unconfined (3d) density flows. It will leverage the experiments (SAL) (see section 2.1), using different prolongation lengths from 1 m to 2.5 m as detailed in table 2 for a constant inlet channel width. The preliminary analysis of the experimental data is presented in figure 15. This includes detailed PIV measurements with spatial resolution of 0.25 cm for the vertical scans (Ex-V) in both x and z axis and 0.72 cm for the horizontal scans (Ex-H) in both x and y axis. The images in figure 15 show contour and quiver plots of the velocity fields obtained for a constant channel width of 0.4 with different prolongations. They show qualitatively, clear distinctions in the flow fields with different confinements. There is an observed increase in the length of the low velocity zone as prolongation increases (see figure 15a). Also, the triangular surface pattern gradually disappears as the prolongation L increases in figure 15b. This is logical as the flow becomes increasingly confined. Further analysis is underway to reveal how the confining wall affects the flow processes and the mixing coefficient.

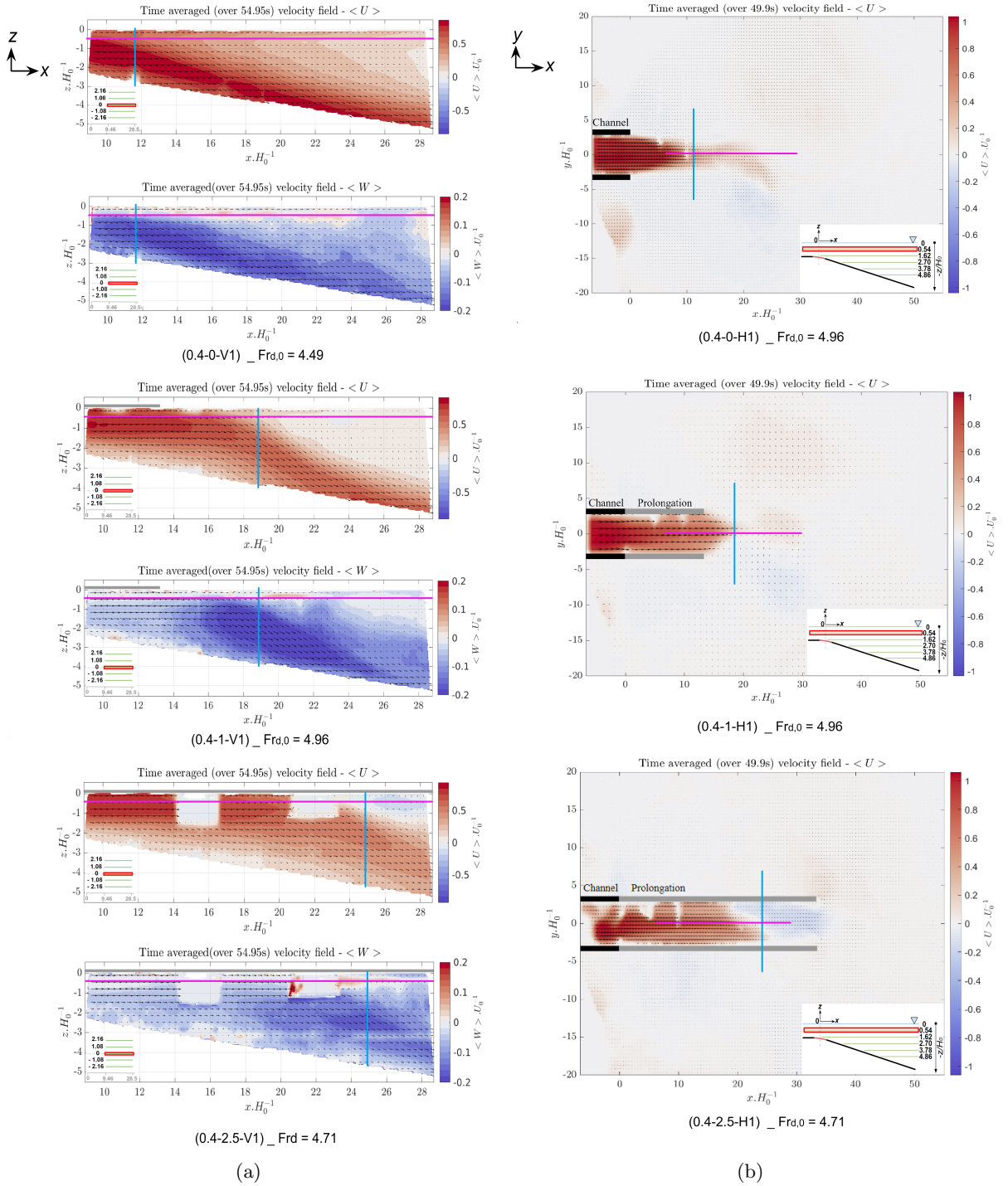

Figure 15: Typical velocity fields for 0 m, 1 m and 2.5 m prolongations respectively from a) Ex-V (mid-scan) and b) Ex-H (at $z = 0.5H_0$). Thick black line represent the extents of the channel. Thick grey line represents the extents of prolongation, green lines are the laser positions with red box indicating the current scan position, light blue lines mark the plunge locations and pink lines represent horizontal laser scan positions on the vertical(Ex-V) slice and vice versa.

Paper 3: The influence of sediment on the flow and mixing processes and the dominant interactions between the flow, sediments and the bathymetry

Kingsley Eze[1], Giamagas George[2], Stan Thorez[1], Eletta Negretti[2],Julien Chauchat[2], Koen Blanckaert[1].

[1]Institute of Hydraulic Engineering and Environmental Hydromechanics, TUWien, Austria.
[2]Laboratoire des Ecoulements Géophysiques et Industriels (LEGI), Grenoble, France.

This paper will address the third and fourth research question (RQ.3 and RQ.4) and their accompanying hypothesis. A series of experiments with depositional end erosional plumes will be performed with informed decisions on the sediment sizes and concentration from the trial experiments described in section 2.2. These experiments will aim to investigate the interaction between the flow, sediments and the bathymetry. Particularly, the important bathymetric variations in the near field region and the feedback due to deposition and re-suspension of sediments.

4 Planning

The proposed project is scheduled to last for 3 years and the progress is tracked in quarters(Q1 to Q4) as shown in figure 16. The first campaign of experiments was concluded in the Q1 of 2024 and the second campaign is scheduled for from the middle of the Q2 of 2025 to the beginning of the Q3 2025.

The data pre-processing phase is nearly complete, with post-processing and analysis currently in progress. These tasks, which are the most time-consuming, are critical to ensuring high-quality results for the planned papers. The writing of the PhD thesis manuscript and the proposed papers is also underway, with the first two papers based on the saline experiments anticipated to be ready for submission by the beginning of Q2, 2025.

In addition to the preparation of these papers, the experiments have been identified as key milestones for the project. Conference attendance and participation in academic courses and seminars are also integrated into the overall plan with the timeline detailed in figure 16.

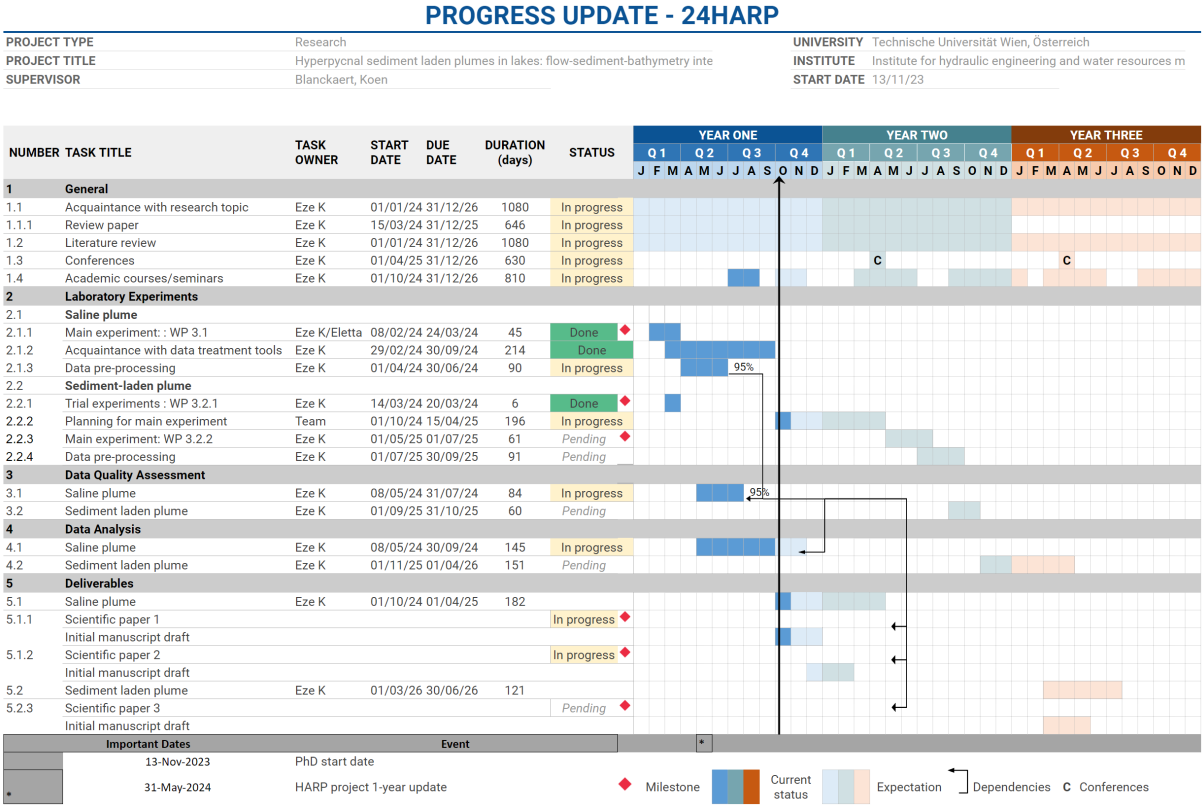

Figure 16: Gantt chart showing the planning and timeline of the PhD

References

Ackers, P. and W. White (1993). "Sediment transport in open channels: Ackers and White update. Technical note." In: *Proceedings of the Institution of Civil Engineers-Water Maritime and Energy* 101.4, pp. 247–249.

Akiyama, J. and H. G. Stefan (1984). "Plunging flow into a reservoir: Theory". In: *Journal of Hydraulic Engineering* 110.4, pp. 484–499.

— (1987). "Onset of underflow in slightly diverging channels". In: *Journal of Hydraulic Engineering* 113.7, pp. 825–843.

Alavian, V., G. H. Jirka, R. A. Denton, M. C. Johnson, and H. G. Stefan (1992). "Density currents entering lakes and reservoirs". In: *Journal of Hydraulic Engineering* 118.11, pp. 1464–1489.

Arita, M. and M. Nakai (2008). "Plunging conditions of two-dimensional negative buoyant surface jets released on a sloping bottom". In: *Journal of hydraulic research* 46.3, pp. 301–306.

Best, A. Kirkbride, and J. Peakall (2001). "Mean flow and turbulence structure of sediment-laden gravity currents: new insights using ultrasonic Doppler velocity profiling". In: *Particulate gravity currents*, pp. 157–172.

Best, R. A. Kostaschuk, J. Peakall, P. V. Villard, and M. Franklin (2005). "Whole flow field dynamics and velocity pulsing within natural sediment-laden underflows". In: *Geology* 33.10, pp. 765–768.

Blanckaert, K., L. R. Vinnå, D. Bouffard, U. Lemmin, and D. A. Barry (2024). "Field observations reveal how plunging mixing and sediment resuspension affect the pathway of a dense river inflow into a deep stratified lake". In: *Water Resources Research* 60.4, e2023WR036813.

Crookshanks, S. and R. Gilbert (2008). "Continuous, diurnally fluctuating turbidity currents in Kluane Lake, Yukon Territory". In: *Canadian Journal of Earth Sciences* 45.10, pp. 1123–1138.

De Leeuw, J., J. T. Eggenhuisen, and M. J. Cartigny (2016). "Morphodynamics of submarine channel inception revealed by new experimental approach". In: *Nature communications* 7.1, p. 10886.

Fischer, H. B. (1979). *Mixing in inland and coastal waters*. Academic press.

Fischer, H. B. and R. D. Smith (1983). "Observations of transport to surface waters from a plunging inflow to lake mead 1". In: *Limnology and Oceanography* 28.2, pp. 258–272.

Fleenor, W. E. (2001). *Effects and control of plunging inflows on reservoir hydrodynamics and downstream releases*. University of California, Davis.

Garcia, M. (1994). "Depositional turbidity currents laden with poorly sorted sediment". In: *Journal of hydraulic engineering* 120.11, pp. 1240–1263.

Garcia, M. and G. Parker (1993). "Experiments on the entrainment of sediment into suspension by a dense bottom current". In: *Journal of Geophysical Research: Oceans* 98.C3, pp. 4793–4807.

García, M. H. (1993). "Hydraulic jumps in sediment-driven bottom currents". In: *Journal of Hydraulic Engineering* 119.10, pp. 1094–1117.

Hage, S., M. J. Cartigny, E. J. Sumner, M. A. Clare, J. E. Hughes Clarke, P. J. Talling, D. G. Lintern, S. M. Simmons, R. Silva Jacinto, A. J. Vellinga, et al. (2019). "Direct monitoring reveals initiation of turbidity currents from extremely dilute river plumes". In: *Geophysical Research Letters* 46.20, pp. 11310–11320.

Hallworth, M. A., A. J. Hogg, and H. E. Huppert (1998). "Effects of external flow on compositional and particle gravity currents". In: *Journal of Fluid Mechanics* 359, pp. 109–142.

Hogg, C. (2014). "The flow of rivers into lakes: experiments and models". PhD thesis. University of Cambridge DAMTP, Cambridge University press, UK.

Hogg, C., C. L. Marti, H. E. Huppert, and J. Imberger (2013). "Mixing of an interflow into the ambient water of Lake Iseo". In: *Limnology and Oceanography* 58.2, pp. 579–592.

Johnson, T. R., C. R. Ellis, and H. G. Stefan (1989). "Negatively buoyant flow in diverging Channel, IV: Entrainment and dilution". In: *Journal of Hydraulic Engineering* 115.4, pp. 437–456.

Lamb, M. P., B. McElroy, B. Kopriva, J. Shaw, and D. Mohrig (2010). "Linking river-flood dynamics to hyperpycnal-plume deposits: Experiments, theory, and geological implications". In: *GSA Bulletin* 122.9-10, pp. 1389–1400.

Lee, H.-Y. and W.-S. Yu (1997). "Experimental study of reservoir turbidity current". In: *Journal of Hydraulic Engineering* 123.6, pp. 520–528.

Mulder, T. and J. P. Syvitski (1995). "Turbidity currents generated at river mouths during exceptional discharges to the world oceans". In: *The Journal of Geology* 103.3, pp. 285–299.

Piton, V., F. Soulignac, U. Lemmin, B. Graf, H. K. Wynn, K. Blanckaert, and D. A. Barry (2022). "Tracing unconfined nearfield spreading of a river plume interflow in a large Lake (Lake Geneva): Hydrodynamics, suspended particulate matter, and associated fluxes". In: *Frontiers in Water* 4, p. 943242.

Sequeiros, O. E., H. Naruse, N. Endo, M. H. Garcia, and G. Parker (2009). "Experimental study on self-accelerating turbidity currents". In: *Journal of Geophysical Research: Oceans* 114.C5.

Sequeiros, O. E., B. Spinewine, R. T. Beaubouef, T. Sun, M. H. Garcia, and G. Parker (2010). "Bedload transport and bed resistance associated with density and turbidity currents". In: *Sedimentology* 57.6, pp. 1463–1490.

Shi, H., M. E. Negretti, J. Chauchat, K. Blanckaert, U. Lemmin, and D. Barry (2024). "Tracking the nearfield evolution of an initially shallow, neutrally buoyant plane jet over a sloping bottom boundary". In: *Water Resources Research* 60.4, e2023WR034826.

Shi, H., M. Negretti, J. Chauchat, K. Blanckaert, U. Lemmin, and D. A. Barry (2022). "Unconfined plunging of a hyperpycnal river plume over a sloping bed and its lateral spreading: Laboratory experiments and numerical modeling". In: *Water Resources Research* 58.8, e2022WR032633.

Shinneeb, A.-M., G. Nasif, and R. Balachandar (2021). "Effect of the aspect ratio on the velocity field of a straight open-channel flow". In: *Physics of Fluids* 33.8.

Singh, B. and C. Shah (1971). "Plunging phenomenon of density currents in reservoirs". In: *La Houille Blanche* 1, pp. 59–64.

Soulignac, F., U. Lemmin, S. M. H. Ziabari, H. K. Wynn, B. Graf, and D. A. Barry (2021). "Rapid changes in river plume dynamics caused by advected wind-driven coastal upwelling as observed in Lake Geneva". In: *Limnology and Oceanography* 66.8, pp. 3116–3133.

Spigel, R. H., C. Howard-Williams, M. Gibbs, S. Stephens, and B. Waugh (2005). "Field calibration of a formula for entrance mixing of river inflows to lakes: Lake Taupo, North Island, New Zealand". In: *New Zealand Journal of Marine and Freshwater Research* 39.4, pp. 785–802.

Stefan, H. G. and T. R. Johnson (1989). "Negatively buoyant flow in diverging channel. III: Onset of underflow". In: *Journal of Hydraulic Engineering* 115.4, pp. 423–436.

Thorez, S., U. Lemmin, D. A. Barry, and K. Blanckaert (2024). "Hydro-sedimentary processes of a plunging hyperpycnal river plume revealed by synchronized remote imagery and gridded current measurements". In: *Water Resources Research* 60.3, e2023WR035907.

Wells, M. G. and R. M. Dorrell (2021). "Turbulence processes within turbidity currents". In: *Annual Review of Fluid Mechanics* 53.1, pp. 59–83.